Available online at www.sciencedirect.com
ScienceDirect
Ceramics International 34 (2008) 531–535
CERAMICS INTERNATIONAL
www.elsevier.com/locate/ceramint

Characterization of partially densified 3D C_f/SiC composites by using mercury intrusion porosimetry and nitrogen sorption

Wei Li *, Zhao-Hui Chen

State Key Laboratory of Advanced Ceramic Fibers & Composites, College of Aerospace and Materials Engineering, National University of Defense Technology, Changsha 410073, PR China

Received 9 October 2006; received in revised form 20 October 2006; accepted 27 November 2006
Available online 13 January 2007

Abstract

The microstructure of partially densified three-dimensional carbon fiber fabrics reinforced silicon carbide (C_f/SiC) composites are characterized by both mercury intrusion porosimetry (MIP) and isothermal nitrogen sorption (INS). By comparison, MIP is preferable to the characterization for its wide effective probing ranges. Based upon multiple measurements, in the C_f/SiC composite, exists a complicated three-dimensional porous network formed by the interconnecting pores and necks with various sizes, diverse shapes and rough surfaces.

Keywords: C_f/SiC composite; Microstructures; Pore network; Mercury intrusion; N_2 sorption

1. Introduction

Carbon fibers reinforced silicon carbide (C_f/SiC) composites have been considered as one of the promising materials for various high temperature structural applications, e.g. aviation and aerospace, transportation system, energy production and chemical engineering, etc. [1–3]. Therefore, great efforts have being made to the R&D of C_f/SiC composites for decades, especially the continuous carbon fibers' fabrics reinforced ones.

Precursor infiltration and pyrolysis (PIP) is one of the most important fabrication processes for C_f/SiC composites, distinguished by its lower fabrication temperatures, simpler facilities and more feasibilities to produce components with complicated shapes. Due to the mass pyrolysis gas escaping and incomplete precursor infiltration, there are inevitably many microvoids and cracks in the interior of PIP fabricated C_f/SiC even after several PIP cycles, as shown in Fig. 1. This specific microstructure determines their mechanical and thermal properties, hence the characterization of it is valuable. Most previous evaluations of C_f/SiC composites were carried out by SEM images analysis [4], but it might be difficult to evaluate overall the materials' bulk quantitatively, because it analyzed two-dimensional limited fields only. Mercury intrusion porosimetry (MIP) and isothermal nitrogen sorption (INS) are classic methods for porous materials evaluation [5]. In this work, the above two approaches are used to characterize PIP-C_f/SiC composites, further microstructure information, besides surface area and pore size distribution (PSD), was obtained referring to the other porous materials' cases.

2. Experimental

The samples were produced through subjecting three-dimensional (3D) carbon fibers fabrics (T300, Toray Inc., Japan) to some infiltration–pyrolysis cycles, using polycarbosilane (PCS) as the precursor. The obtained 3D C_f/SiC composite had been incompletely densified. The morphology of samples' cross-section were characterized by SEM (JSM-5600LV, JEOL). Mercury intrusion porosimetry (AutoporeIII9420 (Micrometics, US)) assumed that the contact angle of Hg on the samples is 130°, and its surface tension is 0.485 N/m. The nitrogen sorption data were gathered by Autosorb-1 (Quantachrome Inc., USA) at 77 K.

3. Theory

3.1. Mercury intrusion porosimery (MIP)

Mercury intrusion is a popular method employed to evaluate porous materials microstructures. Conventional interpretations

* Corresponding author. Tel.: +86 731 4576441; fax: +86 731 4573165.

0272-8842/$34.00
doi:10.1016/j.ceramint.2006.11.015

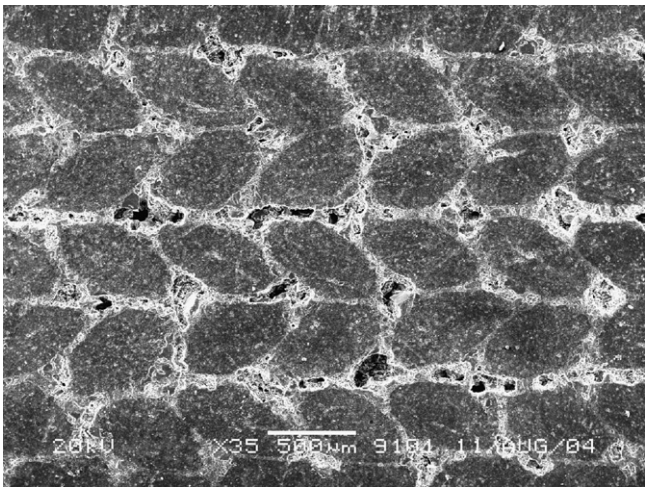

Fig. 1. SEM photo of 3D C_f/SiC composite's cross-section, note the obvious pore chambers and throats inside the bulk.

of original MIP data include porosity, density, and pore size distribution (PSD), etc. Besides these, other structural factors have also been determined based on some calculation models, such as:

3.1.1. Surface area

Surface area is a critical characteristic for porous materials. With the assumption that the contours of pores and channels are uniform, surface area S_w of open pores and connecting channels can be calculated by integrating the P–V curve of mercury intrusion branch, according to the expression as follows [6]:

$$S_w = \frac{1}{\sigma M \cos\alpha} \int_0^{V_{max}} P \, dV \tag{1}$$

where P, M, α, V is the intrusion pressure, sample's mass, contact angle and intruded mercury volume, respectively.

3.1.2. Fractal dimension

Fractal dimension (D) is a parameter to characterize the self-likeness degree of porous solids' microstructure. Owing to their great roughness and high distributing irregularity of pores, the porous materials have a much bigger D than ideal dense ones, undoubtedly. To calculate D from MIP, an expression is deduced from fractal theories and Washburn equation as follows [7]:

$$\log\left(\frac{dV}{dP}\right) = \log(k_2) + (D-4)\log P \tag{2}$$

where P is the intrusion or extrusion pressure, V the corresponding cumulative volume and k_2 is the constant. Hence, D values can be derived from $\log(dV/dP)$ versus $\log P$ plots.

3.2. Isothermal nitrogen sorption (INS)

Also an intruding approach, INS method measures the N_2 adsorption/desorption volumes of the sample at different pressures, from which one can get structural information, e.g. the surface area can be calculated as following [8]:

$$S = 4.36 V_m \tag{3}$$

where V_m is obtained by B.E.T. equation:

$$\frac{x}{V(1-x)} = \frac{1}{V_m C} + \frac{C-1}{V_m C} x, \quad x = \frac{P}{P_0} \tag{4}$$

The pore size distribution can be got based on Barrett–Joyner–Halenda (B.J.H.) model; and fractal dimension can be calculate by Frenkel–Halsey–Hill (F.H.H.) model [9]:

$$\ln\left(\frac{V}{V_m}\right) = \text{const.} + S \ln\left(\ln\left(\frac{P_0}{P}\right)\right) \tag{5}$$

where

$$S = \begin{cases} \dfrac{D-3}{3} & \text{at low pressures} \\ D-3 & \text{at high pressures} \end{cases}$$

Besides F.H.H., Song et al. [10] deduced the B.E.T. equation using to calculate D at low pressures, according to Friat's B.E.T. model:

$$\frac{1}{A} - \frac{1}{2^{2-D} C} \left[\frac{1}{x} + (C-1)\right] \tag{6}$$

where

$$A = \frac{1}{x}\left[\frac{V}{V_m} - \frac{Cx}{1+(C-1)x}\right]$$

4. Results and discussions

4.1. N_2 sorption isotherm and mercury intrusion curve

The N_2 sorption isotherm and mercury intrusion curves of the 3D C_f/SiC composite are shown in Figs. 2 and 3, respectively. In Fig. 2, the adsorption branch ascends slowly and continuously with the pressure increases at the beginning, when the relative pressure exceeds 0.8, the curve jumps

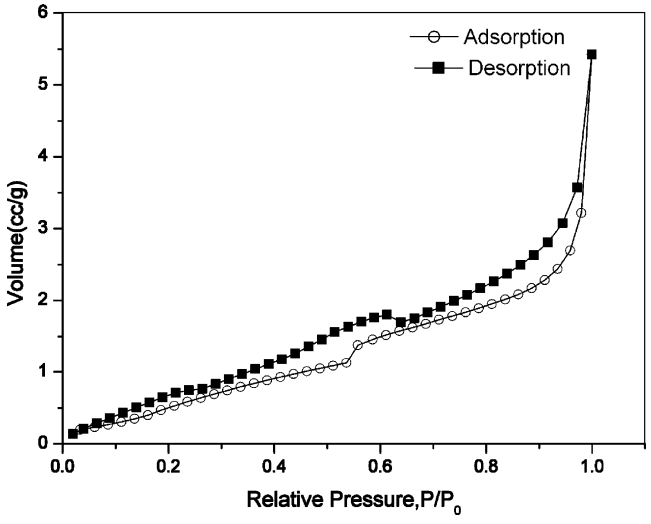

Fig. 2. N_2 sorption isotherm of the 3D C_f/SiC composite.

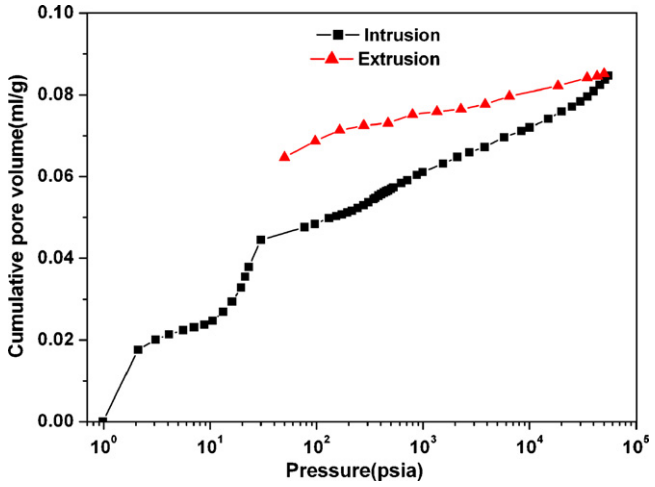

Fig. 3. Mercury intrusion–extrusion curve.

suddenly and straightly, till the adsorption reaches saturation, finally, the whole adsorption branch appears the II isotherm style (by B.E.T. classification). Calculated by B.E.T. equation, the constant C is only 4.25, implying that the enthalpy of adsorption for N_2 on the pores' surfaces is not high, i.e. the adsorbing force of C_f/SiC to N_2 is not strong enough, which is just the reason of the small adsorption volume at low pressures. For the high pressures, it is believed that the sudden increase of adsorption amounts is due to the great quantity and wide size distribution of the pores in the sample, hence while the condensation started, the total entrapped N_2 volume increased greatly. When depressurized, the desorption branch deviates from the adsorption one apparently, and their superposition does not appear until the course ends, which forms a hysteresis loop. This hysteresis loop is not similar to anyone of the five typical styles categorized by de Boer, but is the superpose results of them probably, indicating the complexity of the inner structures and the variety of the pores' shapes.

In Fig. 3, there are two step-like jumps at 70–90 and 3–9 μm, respectively, on the intrusion branch, which shows that pores with size in these ranges have high volume contents, and accommodating much mercury during intrusion. Some also attributes such jumps initiating at 9 μm to the results of the mercury breakthroughs the blocking of the throats interconnecting the pores' chambers, the throats' sizes are 3–9 μm correspondingly [11]. As soon as the pressure descends, the extrusion branch deviates from the intrusion one, which indicates that the small pores shielded by the big ones around them [12]. Unlike the N_2 sorption, the hysteresis of intrusion–extrusion does not form a loop, while at the end of the extrusion, there are still 76 vol.% mercury remained which cannot be withdrawn from the sample. It is well-accepted that this phenomenon is due to the shielding effects of the small pores/necks near the sample surface on the pores/chambers connected with them, that is, during extrusion the mercury flow snap-off in some necks, much mercury drops in the pore chambers are isolated from the main body around the samples and remains inside [13].

In conclusion, in the 3D C_f/SiC composite, a complicated three-dimensional porous network has been formed by lots of pores/throats with various sizes and shapes, connecting and interpenetrating each other.

Table 1
Pore structural data obtained by two approaches

Item	Mercury intrusion	N_2 adsorption
Total pore volume (ml/g)	0.2059[a]	8.386×10^{-3}[b]
Surface area (m^2/g)	12.66	3.41
Median pore radius (volume) (Å)	217,124	–
Median pore radius (area) (Å)	19	–
Average pore radius (Å)	332	51.4
Bulk density (g/cm^3)	1.4009	–
Apparent (skeletal) density (g/cm^3)	1.9687	–
Porosity (%)	28.8412	1.22[c]

[a] Referred to total intrusion volume.
[b] Cumulative pore volume ($P/P_0 < 0.99$).
[c] Calculated from total pore volume as bulk density = 1.45 g/cm^3.

4.2. Pores' basic structural characters

The common structural characters to describe porous medias are listed in Table 1.

By comparison, it is obvious that every item coming from MIP is larger than the one from INS (adsorption) of the same sample, e.g. the former cumulative pore volume is two orders of magnitude larger than the latter, the surface area and average pore radius are four and six times larger, respectively, and also the porosity is much higher than the INS one. That is, the 3D C_f/SiC composite characterized by MIP has more pores in its body with larger sizes and broader distribution. Noticeably, even after five PIP cycles, the composite still possess high porosity (29 vol.%) which is consistent with the previous result obtained from the Archimedes method (25%), moreover, both the bulk and skeletal densities are almost the same.

There are also significant differences in the pore size distribution (PSD) curves derived from MIP and INS, as shown in Fig. 4. The INS result indicates a relatively narrow PSD (Fig. 4(a)): the volumes of pores less than 5000 Å in diameter add up to 76.5% of total, and most of them are between 20 and 1000 Å (2–100 nm), belonging to the nanopores. Below 50 nm, the curve exhibits two peaks at 35.19 and 65.55 Å, respectively, with the area ratio of 3:2.

The pore radius distribution of MIP covers a very wide range from 10 to 10^6 Å, as shown in Fig. 4(b), the whole range can obviously be divided into several regions according to pore volumes' increments, and relative volume of each region as analyzed quantitatively in Table 2.

Different with INS, in the 3D C_f/SiC composite, the micronmeter-scale (1–100 μm) pores are predominant, whose cumulative volumes reach 65.4% of total. These large pores can also be seen clearly in the SEM (Fig. 1). Meanwhile, nanopores (10–1000 Å) also exist, but their total content is less than 10 vol.%, much lower than in the INS case. Interestingly, below 20 nm, the curve exhibits a two-peak feature, too; as the overlapped plot in Fig. 4(b) shows these peaks appear at about 20 and 75 Å, which is consistent with Fig. 4(a).

In summary, for 3D C_f/SiC composite, MIP is an effective approach to characterize comprehensively the porous

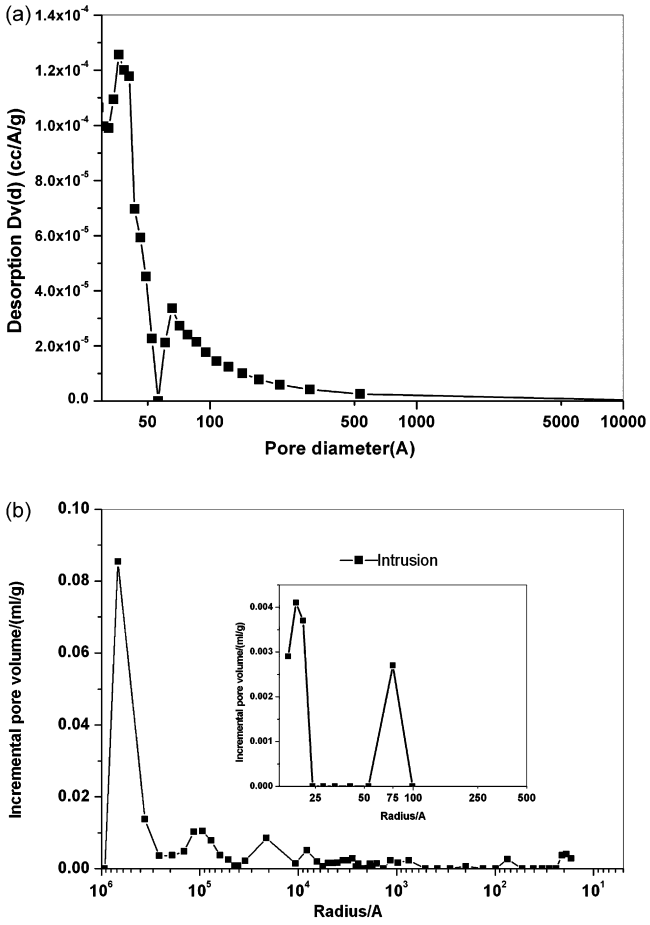

Fig. 4. Pore size distribution (PSD) from: (a) N_2 desorption, and (b) Hg intrusion; the overlapped plot in (b) magnifies the PSD with radius below 200 Å.

Table 2
Relative volumes of pores within main size ranges

Pore size range (Å)	Relative volume (%)
5×10^6–5×10^5	36.9
5×10^5–5×10^4	28.5
5×10^4–1×10^3	21.6
5×10^2–10	7.93

structure, ranging from nanometer scale to micronmeter scale. However, due to its own limitations, INS can hardly distinguish pores with sizes beyond hundreds angstroms, but assigns them to surface and neglects them. Naturally, there are apparent differences between the results of these two approaches.

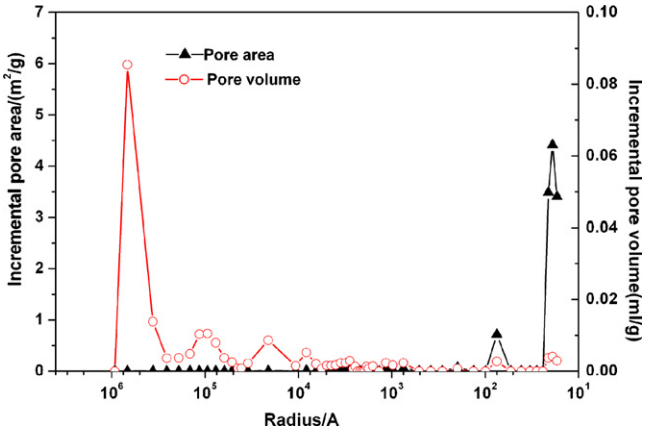

Fig. 5. Plots of pore volume and pore area distributions from MIP.

4.3. Pores' surface features

For porous materials, surface characters also attract great attention. Unlike non-porous materials, pores' formation brings significant changes to the surfaces of porous ones. So is the 3D C_f/SiC composite. Fig. 5 compares the pore size and area distribution curve by MIP. They are obviously different in profile. As the plots indicated, the volume of macropores with size over 1 μm is 65% of total, while their surface area contribution is so small that it can be ignored; contrarily, the relative volume of nanopores below 500 Å is as little as 7.9%, while the area of all pores below 150 Å has reached 96.9% of total. So the surface area of this material is mainly contributed by the mesopores and micropores.

Another factor that describes the surface morphology is fractal dimension D. Both the INS and the MIP data can be used to calculate D, involving many assumptions and models. The choice of a proper model should be determined by considering the fractal theories and actual situation. Furthermore, for the same group of data resulting from each approach, the calculation always produces several different D values. In fact, these D values correlate to various pore size ranges, reflecting their own fractal properties. Our preliminary research by INS shows, at low pressures, that the D calculated by F.H.H. model, Eq. (5), is less than 1, which disobeys the fractal rules; while applying B.E.T. equation, formula (6), brings a more reasonable value (Table 3 and Fig. 6(b)), at high pressures, F.H.H. model is suited for calculation of D, as shown in Table 3 and Fig. 6(a), the regressions both have high linearity. Further analysis supposes that $D_{B.E.T.}$ presents the surface roughness of medium and large pores, while $D_{F.H.H.}$ presents the topological complexity of total pores' configuration. Similarly, for MIP, the

Table 3
Fractal dimensions from N_2 sorption and mercury intrusion

	N_2 adsorption, relative pressure (P/P_0)		Mercury intrusion, pore size (Å)			
Calculation ranges	0.1–0.3	0.75–0.98	5×10^6–5×10^5	5×10^5–5×10^4	5×10^4–1×10^3	5×10^2–10
Calculation methods	B.E.T.	F.H.H.	Formula (2)			
D	2.23	2.789	2.282	2.469	2.682	6.505

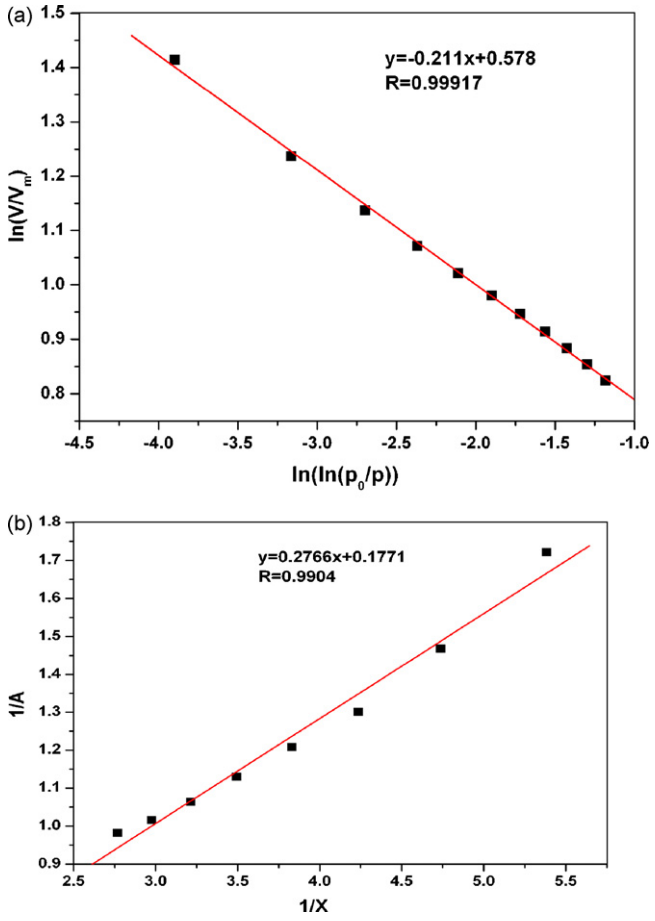

Fig. 6. Regressions to evaluate fractal dimensions from N_2 adsorption data: (a) at high pressure (P/P_0 = 0.75–0.98) by the F.H.H. model, and (b) at low pressure (P/P_0 = 0.1–0.3) by the B.E.T. equation.

D values are different in each pore size range, as shown in Table 3, the smaller the pore size is, the larger the D is, when the size is below 500 Å, formula (2) cannot give reasonable D value. The surface roughness increases with pore size decreasing, which is like the pore surface area distribution in Fig. 5, showing the relationship between the surface area and roughness.

5. Conclusions

The porous structures of incompletely densified 3D C_f/SiC composites fabricated by precursor infiltration–pyrolysis process have been characterized quantitatively by both mercury intrusion porosimetry (MIP) and isothermal N_2 sorption (INS). The results of the two approaches indicate significant differences in porosity, pore size, surface area and PSD, etc.

Our investigation shows that, for 3D C_f/SiC composite, MIP is an effective approach to characterize comprehensively its porous structure, whose sizes ranging from nanometer scale to micronmeter scale and its results are consistent with the ones from other methods, e.g. SEM, the Archimedes method, and even INS. However, in view of its own limitations, INS can hardly distinguish pores with sizes beyond hundreds angstroms, but assigns them to surface and neglects them.

By MIP in partially densified 3D C_f/SiC composite the micron scale-size pores are predominant, whose cumulative volume reaches 65.4% of total; while the nanoscale pores' one is less than 10%.

Intrusion–extrusion and adorption–desorption hysteresis curves implied, that in the 3D C_f/SiC composite, a complicated three-dimensional porous network has been formed by lots of pores/necks with various sizes and shapes, connecting and interpenetrating each other. Ninety-seven percent of the inner surface area of the 3D C_f/SiC composite is contributed by the nanosized pores below 500 Å. Analyzing the intrusion–extrusion and adsorption–desorption data always produces several different D values, which correlate to various pores within different size ranges and reflect rough surface morphology and/or complex topology of pores.

References

[1] U. Papenbrug, S. Beyer, H. Laubeh, et al. Advanced ceramic matrix composites (CMC'S) for space propulsion system. AIAA-1997-3391.
[2] Y. Sanokawa, Y. Ido, Y. Sohda, et al., Application of continuous fiber reinforced silicon carbide matrix composites to a ceramic gas turbine model for automobiles, Ceram. Eng. Sci. Proc. 18 (1997) 221–228.
[3] M. Imuta, J. Gotoh, Development of high temperature materials including CMCs for space applications, Key Eng. Mater. 164/165 (1999) 439–444.
[4] K. Walter, Microstructure tailoring of C/C–SiC composite, Ceram. Eng. Sci. Proc. 24 (2003) 471–476.
[5] D. Lubda, W. Lindner, M. Quaglia, Comprehensive pore structure characterization of silica monoliths, J. Chromatogr. A 1083 (2005) 14–22.
[6] P.S. Liu, X.M. Ma, Characterization of porous medias, Metall. Ind. Beijing (2006).
[7] A. Carlos, L. León, New perspectives in mercury porosimetry, Adv. Colloid Interf. Sci. 76/77 (1998) 341–372.
[8] Y.J. Min, Z.Q. Yuan, G.J. Cong, Adsorption and Condensation, 2nd ed., Science, Beijing, 1986.
[9] L.B. Liu, X.H. Wang, Fractal analysis of bentonite porosity using nitrogen adsorption isotherms, J. Chem. Eng. Chin. Univ. 17 (2003) 591–595.
[10] H. Song, S.X. Xin, X. Jun, et al., Inner-pore structure change of Huainan coal char particle during combustion, J. Chem. Ind. Eng. (China) 54 (2003) 107–111.
[11] C.F. Lorenzano-Porras, et al., Pore structure and diffusion tortuosity of porous ZrO_2, J. Colloid Interf. Sci. 170 (1995) 299–307.
[12] G.R. Wang, Study on pore structure of porous materials under diffusion/reaction conditions, PhD Thesis, Tianjing University, Tianjing, 2000.
[13] F. Porcheron, P.A. Monson, M. Thommes, Molecular modeling of mercury porosimetry, Adorption 11 (2005) 325–329.